Northumbria Research Link

www.northumbria.ac.uk/nrl

northumbria
UNIVERSITY NEWCASTLE

A Novel Equivalent Circuit Model for Split Ring Resonator with an Application of Low Phase Noise Reference Oscillator

Naci Pekçokgüler[a,*], Günhan Dündar[a], Hamdi Torun[a], Arda D. Yalçınkaya[a]

[a]*Department of Electrical and Electronics Engineering, Bogazici University, Bebek, TR-34342 Istanbul, Turkey*

Abstract

This paper presents physical lumped element models for the structures employing a split-ring resonator (SRR) coupled with a pair of microstrip antennas. The results of 3D EM simulations, circuit simulations and measurement results are provided. For experimental verification, a resonator device was fabricated on an FR4 epoxy glass substrate. Mismatch between the values of resonant frequency that are predicted by the models and that are measured is less than 3%. As a benchmarking case for the proposed model, a reference oscillator was designed and implemented. A phase noise of $-139.51\,\mathrm{dBc/Hz}$ at $3\,\mathrm{MHz}$ frequency offset was measured with a center frequency of $1.617\,\mathrm{GHz}$.

Keywords: Metamaterial, split-ring resonator (SRR), equivalent circuit model, electromagnetic simulation, microwave oscillator

1. Introduction

Reference oscillators are among the main building blocks in many electronic systems such as wireless communication systems [1], microprocessors [2], and sensors [3]. A frequency selective network is essential in oscillator design to determine the oscillation frequency. Resonators are usually used as the frequency selective networks. The higher the quality factor of the resonator, the better the performance of the oscillator. Recently, metamaterial-based resonators have been demonstrated as low cost and high quality resonators. Metamaterials provide the opportunity to create engineered structures, which resulted in utterly different applications, such as telecommunication [4], energy harvesting [5], sensing [6], and medical instrumentation [7]. Metamaterials interact with electromagnetic waves and can be used to control or detect them.

Split Ring Resonator (SRR) and its dual, Complementary Split Ring Resonator (CSRR), are widely used structures in metamaterial aplications. They offer a very high $Q-$factor, and exhibit high sensitivity to capacitive and inductive changes in the environment. An electrical lumped element model for these resonators is needed for effective design of circuits and systems. For this model to be used in the design process, it should also include the effects of other parts of the structure which can be transmission lines or antennas to excite resonators. An accurate
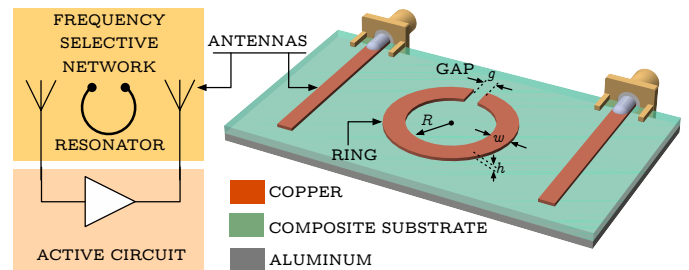

Figure 1: Split Ring Resonator (SRR) structure with planar antennas.

lumped-element model for a CSRR loaded transmission line is provided in [8]. However, the targeted structure in this paper is an antenna-coupled SRR and the discussion will continue with its modeling hereafter. Analytical formulation for calculation of effective capacitance and inductance of the SRRs is given in the literature [9]. Lumped element models for SRRs and SRR loaded transmission lines have been demonstrated before [10, 11, 12]. Calculated capacitance and inductance values can be used in these models. Improvements to the former lumped element models were also presented [13, 14]. These models are based on basic LC resonators with some improvements and the addition of a transmission line model. However, in addition to parameter fitting, which requires a priori information, excessive calculations are needed before using these models in a design. Furthermore, neither of them provide a direct connection between the physical dimensions of the resonator structure and the equivalent model. In addition, the whole structure including both the SRR and the effects of antennas which are used to excite the SRR have not been modeled, yet. The model proposed

---

*Corresponding author at: Department of Electrical and Electronics Engineering, Bogazici University, Bebek, TR-34342 Istanbul, Turkey. Tel.: +90 212 3597368

Email addresses: `naci.pekcokguler@boun.edu.tr` (Naci Pekçokgüler), `dundar@boun.edu.tr` (Günhan Dündar), `hamdi.torun@boun.edu.tr` (Hamdi Torun), `arda.yalcinkaya@boun.edu.tr` (Arda D. Yalçınkaya)

(a)

(c)

(b)

(d)
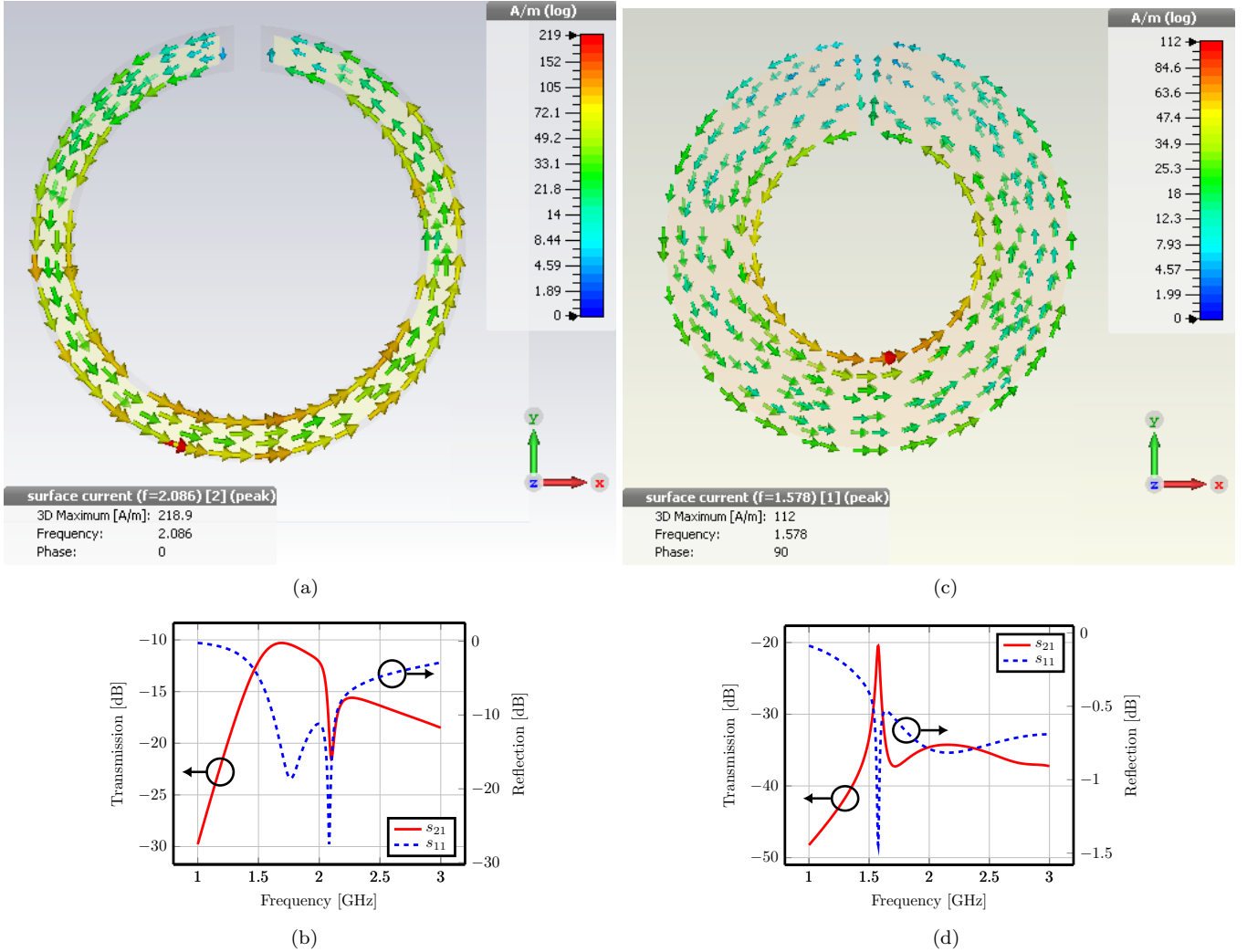
Figure 2: (a) Simulation of surface current density, (b) reflection (S_{11}) spectrum, and transmission (S_{21}) spectrum of the device without backplate, and (c) simulation of surface current density, (d) reflection (S_{11}) spectrum, and transmission (S_{21}) spectrum of the device with backplate.

in this paper addresses this bottleneck, as it consists of parameters which are directly obtained from dimensions of the resonator structure and properties of the materials used in the structure and includes the effects of antennas.

This paper presents a lumped model for an antenna-coupled Split-Ring Resonator, and an oscillator utilizing the resonator. Foundation of the model and its components described in Section 2. Experimental results and their comparison with the equivalent model are provided in Section 3. Section 4 provides the verification of the model used in a reference oscillator benchmark. Finally, results and achievements are discussed in Section 5.

2. Modeling

2.1. Electromagnetic Simulations

Fig.1 shows the structure, which comprises a metallic ring resonator and a set of microstrip antennas implemented on the same plane. Resonator has an inner

ring radius of R, circular metal path having width of w, a thickness of h and a gap of g. The resonator has inductive component due to current being carried by the series path of the metallic ring and two capacitive constituents stemming from the gap and the charge distribution on the metal surface. Two different configurations of the same resonator architecture are considered: a structure with an Aluminum back plate and a structure without any backplate.

The electromagnetic behavior of the SRR structure with an inner radius of $R = 8\,\text{mm}$, a width of $w = 1.25\,\text{mm}$, and a gap of $g = 2.4\,\text{mm}$ is simulated using a commercially available electromagnetic solver (CST Microwave Studio, Darmstadt Germany). Fig.2 (a) shows the surface current density at the resonant frequency (2.1 GHz) of the SRR with no backplate, revealing a circulating current in counter-clockwise direction. Fig.2 (b) shows the reflection (S_{11}) and transmission (S_{21}) spectra, which reveal notches at the resonant frequency.

2

A similar resonator device having dimensions of $R = 6.85\,\text{mm}$, $w = 4\,\text{mm}$, $g = 1.65\,\text{mm}$ is designed to target a lower resonant frequency. This specific device is configured to have a 2 mm-thick aluminum plate on the backside. Fig.2 (c) shows the surface current density distribution at the resonance, exhibiting a circulating current in the counter-clockwise direction. The magnetic resonance frequency formed by the circulating current leads to a dip and a peak in reflection and transmission spectra, respectively as shown in Fig.2 (d). This current results in charge concentration across the gap. In addition to the magnetic field energy concentrated in the region enclosed by the ring, the electric field, which is created due to the charges across the gap, results in energy storage. Thus, the device shows a resonant characteristic to the perpendicular magnetic field [15]. As can be seen from the EM simulation results, device with a metallic backplate has a peak in the transmission spectra, whereas the device without backplate has a dip at resonance. The difference necessitates a specific equivalent circuit model for each configuration.

2.2. Lumped Component Modeling

The resonance behavior of single split-ring resonator can be modelled as a lumped LC circuit as described in [10]. The values of effective inductance and capacitance can be calculated using the following formulas as described in [9]. The total inductance is given as,

$$L_{\text{tot}} = \mu_0 \left(R + \frac{w}{2} \right) \left(\log \frac{8 \left(R + \frac{w}{2} \right)}{h + w} - \frac{1}{2} \right) \qquad (1)$$

where, μ_0 is free-space permeability. The total capacitance is;

$$C_{\text{tot}} = C_{\text{gap}} + C_{\text{surf}} \qquad (2)$$

where, C_{gap} is the gap (split) capacitance, C_{surf} is the surface capacitance and these capacitances are calculated as,

$$C_{\text{gap}} = \varepsilon_0 \frac{hw}{g} + C_0 \quad , \quad C_0 = \varepsilon_0 \left(h + w + g \right) \qquad (3)$$

$$C_{\text{surf}} = \frac{20 \varepsilon_0 \left(h + w \right)}{\pi} \log \frac{4R}{g} \qquad (4)$$

where, ε_0 is free-space permittivity, and C_0 is the correction to the parallel plate capacitance due to the fringe fields. The resonant frequency is calculated as;

$$f_0 = \frac{1}{2\pi \sqrt{L_{\text{tot}} C_{\text{tot}}}} \qquad (5)$$

Using the design geometries, equivalent inductance and capacitance values of the SRR used in backplate configuration are calculated as $L_{\text{tot}} = 26.3\,\text{nH}$ and $C_{\text{tot}} = 392\,\text{fF}$. The resultant resonant frequency of this device is $f_0 =$
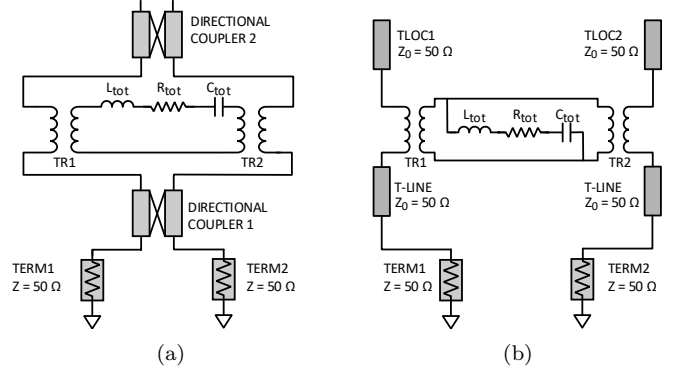

Figure 3: Proposed model equivalent circuit schematic for (a) the device with backplate, (b) the device without backplate.

1.6 GHz. For the the SRR with no backplate equivalent parameters are calculated as $L_{\text{tot}} = 37.8$ nH and $C_{\text{tot}} = 161\,\text{fF}$, respectively. This device has a calculated resonant frequency of $f_0 = 2\,\text{GHz}$.

Once the effective capacitance and inductance values of the structure are calculated by using physical dimensions, these values can be directly used in the LC model to emulate the core of the resonator. However, SRRs are typically used in applications where they are embedded with other passive elements such as transmission lines and antennas. Moreover, when a filter or an oscillator application is aimed, an interface between the overall network of the resonator, including peripheral passives, and the active circuitry must be constructed. Therefore, the complete response of the network including antennas and transmission lines is needed.

2.2.1. SRR with a Backplate

In this configuration, the aluminum backplate converts the microstrip lines into open circuited microstrip stubs. When the structure is examined in the absence of SRR, it can be considered as a microstrip coupled line directional coupler with open circuited through and isolated ports, and the coupled port is the second port in our structure. However, this approach is just used to model the structure. It does not suggest that the physical structures are the same as the components used in the model. Since the spacing between the lines is very large, coupling is very weak. When the SRR is added to the structure, it transfers power between lines, and a peak is observed in transmission spectrum at resonance. Off-resonance transmission will be very low.

When this operation principle is considered, the model should contain a coupled line directional coupler, an RLC resonator, and a magnetic coupling between these two circuits. The proposed lumped element model for this structure is depicted in Fig. 3(a), where R_{tot}, L_{tot}, and C_{tot} form the core of the resonator. Values of the L_{tot} and C_{tot} are calculated by using equations (1) and (2), respectively. At the resonance, equivalent impedance converges to the value of R_{tot}, which controls the quality factor of
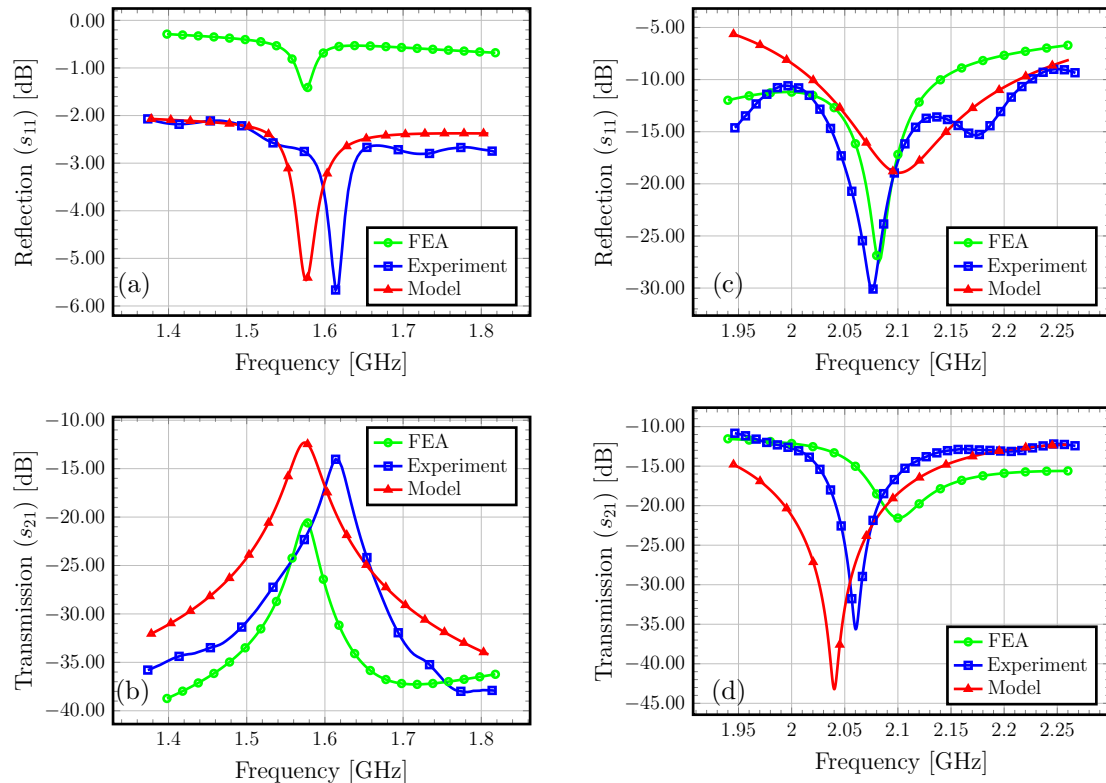
Figure 4: (a) Reflection (S_{11}) spectrum, (b) transmission (S_{21}) spectrum of the device with backplate for all the cases, (c) reflection (S_{11}) spectrum, (d) transmission (S_{21}) spectrum of the device without backplate for all the cases.

the resonator. RLC resonator is connected in series with the signal path, thereby, transmission is ensured solely in vicinity of the resonance band. $50\,\Omega$ microstrip coupled lines (Directional coupler-1) model the antennas having equal lengths. Isolated and through ports of Directional Coupler-2 are left open circuit to obtain the open-end effect in the antennas. Ideal transformers (TR1 and TR2) are added to the model to include the magnetic coupling between the resonator and the antennas. These transformers are placed between the directional couplers and the resonator core, to emulate the physical layout of the resonator with respect to the antennas. Coupling coefficient of the transformer is used as a fit parameter in the model, and it has no effect on the resonant frequency. It just determines the ratio of power transmitted to the resonator, thus, the magnitude of the peak in the transmission.

2.2.2. SRR without a Backplate

In the absence of the back plate, microstrip lines behave as monopole antennas. Fair amount of transmission occurs between the antennas around the resonant frequency of the antennas. In order to model the transmission notch given in Fig. 2 (b), a parallel RLC path, which reduces transmission to a significantly low value, is introduced.

Fig. 3 (b) shows the proposed equivalent circuit model for the device without a backplate. The series resonance

circuit composed of R_{tot}, L_{tot} and C_{tot} blocks the transmission of a specific frequency band designed by the ring resonator geometry. In this model, TL1 and TL2 are microstrip transmission lines, and TLOC1 and TLOC2 are open circuit microstrip stubs, all having $50\,\Omega$ characteristic impedance. The total length of TL1 and TLOC1 is equal to the length of antennas in the network as well as the total length of TL2 and TLOC2. Since the network is reciprocal, lengths of TL1 and TL2 and lengths of TLOC1 and TLOC2 are equal to each other. TLOCs include the open-end effects. Ideal transformers model the magnetic coupling between the resonator and antennas. The properties of transformers and their locations between the microstrip lines are the same as the former model.

3. Experimental Verification of the Model

The resonator with the antenna pair network is implemented on a $1.57\,\mathrm{mm}$-thick FR4 epoxy-glass substrate ($\varepsilon_r = 4.4$) with a copper thickness of $35\,\mu\mathrm{m}$. Transmission and reflection spectra are obtained by using two-port measurements with a Vector Network Analyzer-VNA (Rohde and Schwarz ZVB4) in vicinity of resonance frequency. Fig. 4 shows s-parameters obtained from finite element analysis (FEA), VNA measurements and lumped element equivalent circuit model simulations, for each configuration. According to the FEA results, the device with
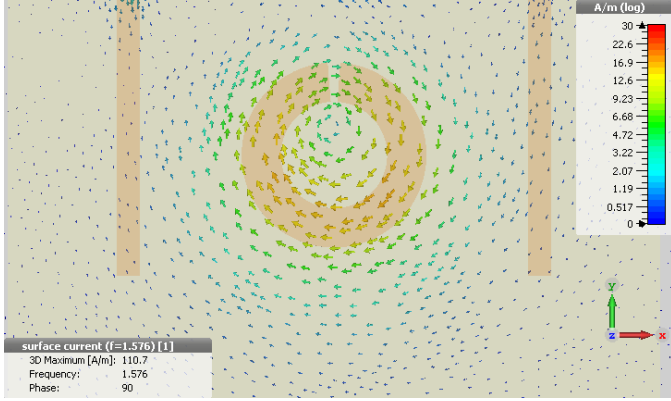
Figure 5: Simulation of surface current density of Aluminum backplate.

the backplate exhibits a resonant frequency at 1.576 GHz, where a circulating current is formed in the ring. This behavior is verified through VNA measurements, giving $f_0 = 1.617$ GHz with a Q-factor of 57.6, leading to a relative difference of 2.5% compared to FEA. The model given in Fig. 3(a) is constructed by using parameter values that are extracted from the design geometries. Simulation of the model estimates a resonant frequency of 1.574 GHz, which is within an error margin of 3%, both respect to FEA and experiments.

The device with no backplate reveals a FEA simulated and experimentally obtained resonant frequencies of 2.1 GHz and 2.06 GHz with a Q-factor of 343.2, respectively. The model given in Fig. 3(b) with parameters calculated from the physical dimensions of the device predicts the resonant frequency as 2.04 GHz. The mismatch between the measured and modeled resonant frequencies is less than 1%. In addition to ability of inclusion of purely physical parameters calculated directly from the design, proposed models have very high accuracy in determining the resonant frequencies of the resonators.

The devices used in this work were fabricated on a standard FR4 epoxy glass substrate. Photolithography was used in the fabrication. As a natural result of fabrication process, there appears some alterations between the layout dimensions and the fabricated structure. Main factors cause these differences are the mask generation, photoresist development and etching processes. These dimension changes in the fabricated devices directly affect the resonant frequency of the structures as formulated in equations 1, 3, 4, and 5. In the proposed model calculations and FEA simulations, drawn layout dimensions were used. This causes the error between the measurements and models. SRR structure is very sensitive to these dimensions, thus errors up to 3% in resonant frequency determination were observed. Additionally, used substrate has variations on relative permittivity, loss tangent and physical dimensions form production lot to lot and they all depend on frequency as illustrated in [16]. These varia-

tions result in mismatches at off-resonance. Obviously, the level of agreement between the results of our model, finite element simulations and experiments can be improved using fitting factors to accommodate possible non-idealities in fabrication and other environmental factors. However, authors believe that an important aspect of the proposed model is that it does not rely on any fitting factors in determining the resonant frequency, rather it only depends on the design geometry.

At resonance, there occurs a circulating current on the surface of backplate because of the altering magnetic field in the configuration of device with backplate (see Fig.5). This current flows in the opposite direction of the current flows on the split ring and degrades the overall magnetic flux. This decrease in the magnetic flux results in a degradation in quality factor. Because of this phenomenon, Q-factor of the device with backplate is lower than that of the device with no backplate.

4. Reference Oscillator Application

4.1. Oscillator Design

The oscillator design is based on an amplifier using the high-Q SRR device in the positive feedback loop as a frequency selective network [17]. In order to obtain a sustained oscillation signal, the magnitude of the loop gain must at least equal to unity and the phase shift in the loop must be 0° at the resonant frequency. Since the SRR structure has a high reflection over a wide frequency range,
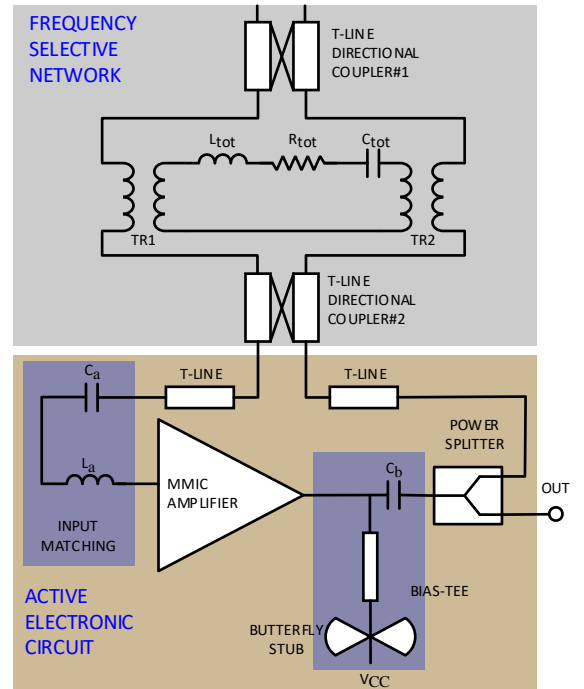

Figure 6: Block level schematic of the oscillator.

5

the circuit may end up with unstable conditions and oscillate at other frequencies than the desired if the amplifier is not designed properly. In order to prevent that, an MMIC amplifier (Avago Tech. MGA86563) with a moderate gain ($G \approx 21$ dB) and high directivity ($S_{12} < -45$ dB) is selected. The SRR structure with a backplate is used in the oscillator design, due to the high-Q peak offered in the transmission spectrum. This peak leads to a minimum loss at the resonant frequency. When this loss is compensated by the active electronic circuit, damping in the loop becomes negative and oscillations start to grow.

The schematic of the oscillator is depicted in Fig. 6. $L_a = 3.3$ nH (EPCOS B82496C3339A) and $C_a = 1$ nF (Murata GRM39COG102J25) are used for input matching. T-LINE represents 3 mm-wide, 35 mm-long additional transmission line between the SRR structure and the amplifier which is used to adjust the phase. Butterfly stub, a quarter-wave transformer and $C_b = 1$ nF (Murata GRM39COG102J25) form the bias-tee structure. -3 dB power splitter (Mini Circuits ZFSC-2-372-S+) is used at the output of the amplifier to obtain the output signal from the oscillator. OUT is read by a 50 Ω-measurement equipment. Power consumption of the circuit with $V_{CC} = 5$ V is measured to be 85 mW. Fig. 7 shows a photograph of the experimental circuit. Metal box is used as a Faraday cage. SRR structure and backplate are placed on top of the box.
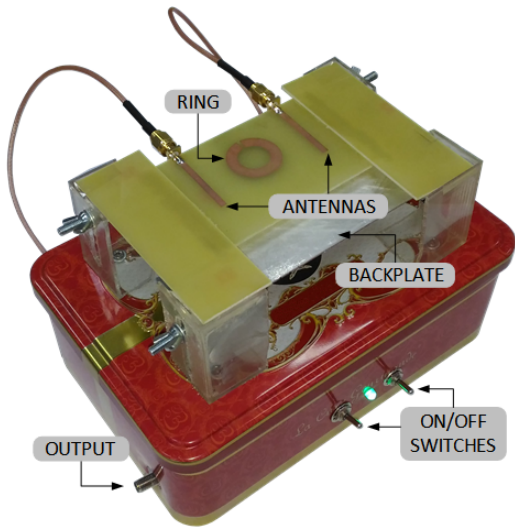

Figure 7: Photograph of the experimental circuit.

4.2. Phase Noise

The oscillator is characterized by time and frequency domain measurements of the output signal. The signal obtained from the oscilloscope (Rohde & Schwarz RTO2034, 3 GHz bandwidth) is given in Fig.8. The voltage excursion is 1.32 V (peak to peak) and the period of the signal is 618 ps. Frequency spectrum of the output is acquired by using a spectrum analyzer (Rohde & Schwarz FSV 30).
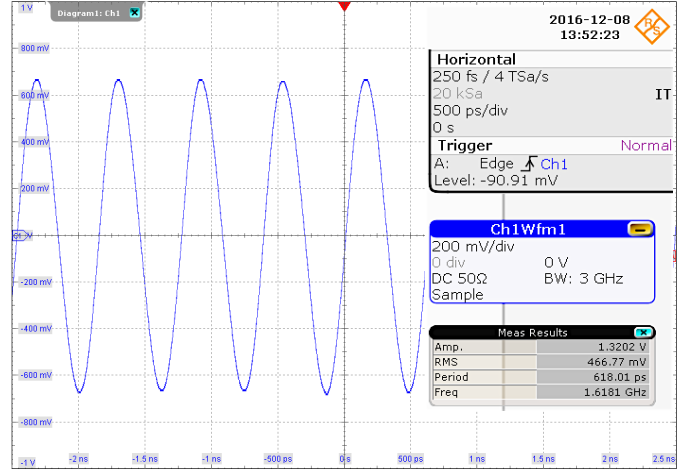

Figure 8: Measured time domain response of the oscillator.

The oscillation frequency is measured as 1.617 GHz, with a carrier power of 6.4 dBm. The phase noise is measured as -139.51 dBc/Hz at the frequency offset of 3 MHz. Variation of the phase noise with respect to offset bandwidth is given Fig.9. The figure of merit (FOM) is calculated as [18]:

$$FOM = L(\Delta f) - 20 \log \left(\frac{f_c}{\Delta f} \right) - 10 \log \left(\frac{P_{DC}}{1\text{mW}} \right) \quad (6)$$

where $L(\Delta f)$ is phase noise at the offset frequency Δf, f_c is oscillation frequency, Δf is the offset frequency, and P_{DC} is the DC power consumption of oscillator. Table 1 summarizes performances of the reported similar oscillators and this work. Oscillators with an oscillation frequency around $1 - 4$ GHz band were listed. [18] outperforms since its oscillation frequency is higher and has better phase noise yet oscillation frequency of reported oscillator in this work can be scaled up via scaling resonant frequency of the SRR with almost no drawback in Q-factor and performance can be improved much further.

Table 1: Comparison of Reported Oscillators

Ref.	f_c [GHz]	$P_D C$ [mW]	L{Δf} [dBc/Hz]	FOM [dBc/Hz]
[18]	4.18	20	-134.2[a]	-192.7
[19]-1	2.675	168	-105.5[b]	-177.1
[19]-2	3.77	161.5	-99.63[b]	-179.9
[20]	3.36	11	-102.86[c]	-132.98
This work	1.617	85	-129.24[a]	-180.5

[a]Phase noise at 1 MHz offset frequency
[b]Phase noise at 100 KHz offset frequency
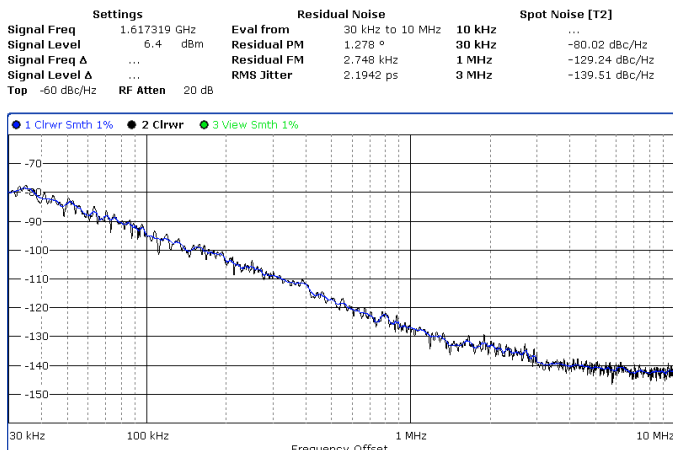[c]Phase noise at 10 MHz offset frequency

Figure 9: Measured phase noise of the microwave oscillator as a function of the offset bandwidth from the carrier.

5. Conclusion

This paper presents a novel lumped element model for ring resonator structures coupled with planar antennas on a single substrate. Accuracy of the model is proven on two sample resonator devices with less than 3% error in the resonant frequency estimation both in reference to 3D electromagnetic solver and experimental measurement results. The lumped equivalent uses purely layout parameters, resulting in an efficient connection between physical structure and the simulation model. A reference oscillator with high spectral purity is developed with the proposed model and -139.51 dBc/Hz phase noise at 3 MHz frequency offset at 1.617 GHz center frequency is achieved with a power consumption of 85 mW. The oscillator delivers a sinusoidal signal with a purity to satisfy Long Term Evolution (LTE) phase noise requirements (-124 dBc at 600 kHz offset bandwidth).

Acknowledgment

References

[1] R. B. Staszewski, P. T. Balsara, Phase-domain all-digital phase-locked loop, IEEE Transactions on Circuits and Systems II: Express Briefs 52 (3) (2005) 159–163. doi:10.1109/TCSII.2004.842067.

[2] D. D. Lee, S. I. Kong, M. D. Hill, G. S. Taylor, D. A. Hodges, R. H. Katz, D. A. Patterson, A vlsi chip set for a multiprocessor workstation. i. an risc microprocessor with coprocessor interface and support for symbolic processing, IEEE Journal of Solid-State Circuits 24 (6) (1989) 1688–1698. doi:10.1109/4.45007.

[3] M. Nalezinski, M. Vossiek, P. Heide, Novel 24 ghz fmcw front-end with 2.45 ghz saw reference path for high-precision distance measurements, in: Microwave Symposium Digest, 1997., IEEE MTT-S International, Vol. 1, 1997, pp. 185–188 vol.1. doi:10.1109/MWSYM.1997.604552.

[4] J. Naqui, G. Zamora, F. Paredes, J. Bonache, F. Martín, Metamaterial transmission lines for wireless communications, sensing and rfid, in: Proceedings of 2014 Mediterranean Microwave Symposium (MMS2014), IEEE, 2014, pp. 1–6.

[5] Z. Chen, B. Guo, Y. Yang, C. Cheng, Metamaterials-based enhanced energy harvesting: A review, Physica B: Condensed Matter 438 (2014) 1–8.

[6] M. J. Freire, R. Marques, L. Jelinek, Experimental demonstration of a $\mu=$- 1 metamaterial lens for magnetic resonance imaging, Applied Physics Letters 93 (23) (2008) 231108.

[7] J. Naqui, M. Durán-Sindreu, F. Martín, Novel sensors based on the symmetry properties of split ring resonators (srrs), Sensors 11 (8) (2011) 7545–7553.

[8] B. Mukherjee, P. Patel, J. Mukherjee, A novel hemispherical dielectric resonator antenna with complementary split-ring-shaped slots and resonator for wideband and low cross-polar applications, IEEE Antennas and Propagation Magazine 57 (1) (2015) 120–128. doi:10.1109/MAP.2015.2397113.

[9] O. Sydoruk, E. Tatartschuk, E. Shamonina, L. Solymar, Analytical formulation for the resonant frequency of split rings, Journal of Applied Physics 105 (1) (2009) 014903.

[10] J. D. Baena, J. Bonache, F. Martin, R. M. Sillero, F. Falcone, T. Lopetegi, M. A. Laso, J. Garcia-Garcia, I. Gil, M. F. Portillo, et al., Equivalent-circuit models for split-ring resonators and complementary split-ring resonators coupled to planar transmission lines, IEEE Trans. Microw. Theory Techn. 53 (4) (2005) 1451–1461.

[11] X. Hu, Q. Zhang, Z. Lin, S. He, Equivalent circuit of complementary split-ring resonator loaded transmission line, Microw. Opt. Technol. Lett. 51 (10) (2009) 2432–2434.

[12] L. Su, J. Naqui, J. Mata-Contreras, F. Martín, Modeling metamaterial transmission lines loaded with pairs of coupled split-ring resonators, IEEE Antennas and Wireless Propagation Letters 14 (2015) 68–71.

[13] F. Aznar, J. Bonache, F. Martín, Improved circuit model for left-handed lines loaded with split ring resonators, Applied Physics Letters 92 (4) (2008) 043512.

[14] R. Bojanic, V. Milosevic, B. Jokanovic, F. Medina-Mena, F. Mesa, Enhanced modelling of split-ring resonators couplings in printed circuits, IEEE Trans. Microw. Theory Techn. 62 (8) (2014) 1605–1615.

[15] J. Zhou1, T. Koschny, C. M. Soukoulis, Magnetic and electric excitations in split ring resonators, Opt. Express Optics Express 15 (26) (2007) 17881–17890.

[16] J. Aguilar, M. Beadle, P. Thompson, M. Shelley, The microwave and rf characteristics of fr4 substrates.

[17] E. J. Post, H. F. Pit, Alternate ways in the analysis of a feedback oscillator and its application, Proceedings of the IRE 39 (2) (1951) 169–174. doi:10.1109/JRPROC.1951.231436.

[18] Z. Yang, J. Dong, B. Luo, T. Yang, Y. Liu, Low phase noise concurrent dual-band oscillator using compact diplexer, IEEE Microwave and Wireless Components Letters 25 (10) (2015) 672–674.

[19] Y. Dong, T. Itoh, A dual-band oscillator with reconfigurable cavity-backed complementary split-ring resonator, in: Microwave Symposium Digest (MTT), 2012 IEEE MTT-S International, IEEE, 2012, pp. 1–3.

[20] B. Iyer, A. Kumar, N. P. Pathak, 3.36-/5.24-ghz concurrent dual-band oscillator for wimax/wlan applications, in: Microwave and RF Conference, 2013 IEEE MTT-S International, IEEE, 2013, pp. 1–4.

Naci Pekcokguler received his B.S. degree from Bogazici University, Istanbul, Turkey in 2016, and is studying for M.S. degree at Bogazici University, all in Electrical and Electronics Engineering. He is research and teaching assistant at the Department of Electrical and Electronics Engineering at Bogazici University. His research interests are analog and RF integrated circuits, and microwave circuit design.

Gunhan Dundar received his BS and MS degrees from Bogazici University, Istanbul, Turkey in 1989 and 1991, respectively, and his PhD degree from Rensselaer Polytechnic Institute, NY in 1993, all in Electrical Engineering. He has been lecturing at Bogazici University since Spring 1994. He was with EPFL, Switzerland between 2002 and 2003, and with TUM, Germany in 2010. He has been holding the professor title since March 2002. His research interests are on analog IC design and electronic design automation.

Hamdi Torun is an associate professor at the Department of Electrical and Electronics Engineering and affiliated with the Center for Life Sciences and Technologies at Bogazici University, Istanbul, Turkey. He received his B.S. degree from Middle East Technical University, Ankara, Turkey, in 2003, his M.S. degree from Koc University, Istanbul, Turkey, in 2005, and his Ph.D. degree from the Georgia Institute of Technology, Atlanta, USA in 2009, all in electrical engineering. He was a postdoctoral fellow in the Department of Mechanical Engineering, Georgia Institute of Technology during 2009-2010. His research expertise is in development of micro/nanosystems for biomedical applications.

Arda D. Yalcinkaya received his B.S. degree from Istanbul Technical University (ITU), Electronics and Telecommunication Engineering Department, Istanbul, Turkey, M.Sc. and Ph.D. degrees from Technical University of Denmark (DTU), Department of Micro and Nano Technology (MIC), Kgs. Lynby, Denmark, all in Electrical Engineering in 1997, 1999 and 2003, respectively. Between 1999 and 2000 he was a research and development engineer at Aselsan Microelectronics, Ankara, Turkey. He had short stays as a visiting reseacher at Interuniversity Microelectronic Center (IMEC), Leuven, Belgium, Centro Nacionale de Microelectronica (CNM), Barcelona, Spain in 2000 and 2003. Between 2003 and 2006, he was a post-doctoral research associate at Koc University, Istanbul. During that period he served as a consultant to Microvision Inc., Seattle, USA. He has been a faculty member of the Department of Electrical and Electronics Engineering, Bogazici University, Istanbul, since 2006, where he is currently an Associate Professor. His research interests include photonics, metamaterials, microelectromechanical systems and analog integrated circuits. Dr. Yalcinkaya was a recipient of the Sabanci Foundation (VAKSA), Turkish Education Foundation (TEV) scholarships during his studies. He received Boazici University Foundation Excellence in Research Award, Middle East Technical University (METU) Mustafa Parlar Foundation Research Encouragement Award, and Turkish Academy of Sciences (TUBA), Distinguished Young Scientists Award (GEBIP) in 2010, 2011, and 2013, respectively.